

# COSMOGRAIL: the COSmological MOnitoring of GRAvltational Lenses I.

## How to sample the light curves of gravitationally lensed quasars to measure accurate time delays.

A. Eigenbrod<sup>1</sup>, F. Courbin<sup>1</sup>, C. Vuissoz<sup>1</sup>, G. Meylan<sup>1</sup>, P. Saha<sup>2</sup>, and S. Dye<sup>3</sup>

<sup>1</sup> Ecole Polytechnique Fédérale de Lausanne, Laboratoire d'Astrophysique, Observatoire, CH-1290 Chavannes-des-Bois, Switzerland

<sup>2</sup> Astronomy Unit, School of Mathematical Sciences, Queen Mary and Westfield College, University of London, Mile End Road, London E1 4NS, UK

<sup>3</sup> School of Physics and Astronomy, Cardiff University, 5 The Parade, Cardiff, CF24 3YB, UK

Received 23 November 2004 / Accepted 16 February 2005

**Abstract.** We use numerical simulations to test a broad range of plausible observational strategies designed to measure the time delay between the images of gravitationally lensed quasars. Artificial quasar light curves are created along with Monte-Carlo simulations in order to determine the best temporal sampling to adopt when monitoring the photometric variations of systems with time delays between 5 and 120 days, i.e., always shorter than the visibility window across the year. Few and realistic assumptions are necessary on the quasar photometric variations (peak-to-peak amplitude and time-scale of the variations) and on the accuracy of the individual photometric points. The output of the simulations is the (statistical) relative error made on the time delay measurement, as a function of **1-** the object visibility over the year, **2-** the temporal sampling of the light curves and **3-** the time delay. Also investigated is the effect of long term microlensing variations which must be below the 5% level (either intrinsically or by subtraction) if the goal is to measure time delays with an accuracy of 1-2%. However, while microlensing increases the random error on the time delay, it does not significantly increase the systematic error, which is always a factor 5 to 10 smaller than the random error. Finally, it is shown that, when the time delay is comparable to the visibility window of the object, a logarithmic sampling can significantly improve the time delay determination. All results are presented in the form of compact plots to be used to optimize the observational strategy of future monitoring programs.

**Key words.** Gravitational lensing: time delay, quasar, microlensing – Cosmology: cosmological parameters, Hubble constant.

### 1. Measuring time delays

Measuring time delays in gravitationally lensed quasars is difficult, but not as difficult as it first appeared in the late 80s when the first monitoring programs were started. Obtaining regular observing time on telescopes in good sites was (and is still) not easy and the small angular separations between the quasar images require to perform accurate photometry of blended objects, sometimes with several quasar images plus the lensing galaxy within the seeing disk.

#### 1.1. COSMOGRAIL

The COSMOGRAIL project (COSmological MOnitoring of GRAvltational Lenses), started in April 2004, addresses

both issues of carrying out photometry of faint blended sources and of obtaining well sampled light curves of lensed quasars. The project involves 5 telescopes: **(1)** the Swiss 1.2m *Euler* telescope located at La Silla, Chile, **(2)** the Swiss-Belgian 1.2m *Mercator* telescope, located in the Canaria islands (La Palma, Spain), **(3)** the 2m robotic telescope of the Liverpool University (UK), also located at La Palma, **(4)** the 1.5m telescope of Maidanak observatory in Uzbekistan, and **(5)** the 2m Himalayan Chandra Telescope (HCT).

All 5 telescopes, and others that will join the collaboration, are used in order to follow the photometric variations of most known gravitationally lensed quasars that are suitable for a determination of  $H_0$ . The sample of targets is described further in Saha et al. (2005), as well as

the non-parametric models and predicted time delays for all of them. Our target accuracy on individual photometric points is 0.01 mag, well within the reach of a 1-2m class telescope and average seeing ( $1''$ ) in a good site. This accuracy is reached even for the blended components of lensed quasars, thanks to image deconvolution algorithms such as the MCS algorithm (Magain et al. 1998).

The results presented in the following were obtained to optimize the observations of the COSMOGRAIL project, which aims at measuring time delays, with an accuracy close to 1% within 2 years of observations (per lensed quasar).

Although large amounts of time are available for COSMOGRAIL on each telescope, optimizing the time spent on each lensed quasar, depending on its luminosity and expected time delay, remains very important. The present paper aims at optimizing the temporal sampling to adopt in order to derive accurate time delays for as many lensed quasars as possible.

The paper is organized in the following way. Section 2 describes how we simulate the light curves of the quasar images. In Section 3, we present which parameters of the simulated light curves are varied and in which range they are varied. In Section 4, we explain how the time delays are extracted from the simulated light curves. The results of these simulations are discussed in Section 5. Since most lensed quasar light curves are probably affected by microlensing events, it is important that our simulations include such effects in order to evaluate their influence on the determination of the time delay. This is treated in Section 6. Finally, Section 7 investigates the effect of logarithmic sampling on the light curves and shows how this irregular sampling can improve the time delay measurements when it is of the order of the visibility window of the object. Note that we consider here only the time delays measured from optical light curves. Radio observations have characteristics that are completely different from the present simulations: noise properties, better spatial resolution, less sensitivity to microlensing.

## 1.2. Which accuracy ?

Not all lensed quasars are suited to an accurate determination of  $H_0$ , first because not all of them have nice lens models with little influence of degeneracies and, second, because the error on the time delay propagates linearly into the error budget on  $H_0$ . While the latter is not the dominant component in the error budget it can (and should) be made almost negligible compared with the other sources of uncertainty. A precision of a few percent should be the goal of the photometric monitoring programs aimed at measuring time delays, if  $H_0$  is to be measured with an accuracy competitive with other methods. So far, very few time delays are known with very high accuracy. Among the best examples are the double Q 0957+561 (Colley et al. 2003), measured in optical wavelengths, and the quadruple B 1608+656 (Fassnacht et al. 2002), measured in radio

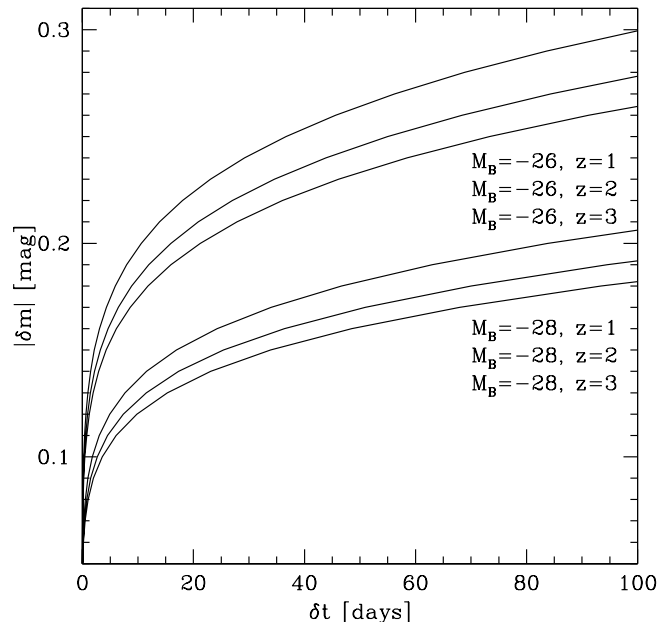


**Fig. 1.** Expected quasar variations  $\delta m$  in magnitudes as a function of the time interval  $\delta t$  (see text). The curves are plotted for 2 different absolute magnitudes  $M_B$  and for 3 quasar redshifts.

wavelengths. Most other lensed quasars have time delays known with a precision of about 10%.

The accuracy of the time delays depends critically on the temporal sampling, on the visibility of the object over the year, on the influence of microlensing, and on the good will of the quasar source to show photometric variations at all. Using numerical simulations on artificial quasar light curves, we try in the present work to define the optimal observational strategy to adopt in order to reach a desired accuracy on the time delay. We consider only the time delay between two quasar images. Our simulations remain applicable to multiple time delays in quads, but the errors on the photometric measurements of the 4 (or more) components must be uncorrelated.

## 2. Simulated light curves

The first step of the process is to generate artificial quasar light curves whose properties mimic quasar variations in a realistic way. A useful benchmark here is the analysis by Hook et al. (1994), of the variability properties of a sample of some 300 quasars.

They find that the variability  $\delta m$  of optically selected quasars can be represented by a function of the form:

$$|\delta m| = (0.155 + 0.023(M_B + 25.7)) \left( \frac{\delta t}{1+z} \right)^{0.18}$$

where  $M_B$  is the absolute  $B$  magnitude,  $z$  is the redshift, and  $\delta t$  is the time interval, in days, over which  $\delta m$  applies. We plot this relation in Fig. 1, for different luminosities ( $M_B = -26, -28$ ), and redshifts ( $z = 1, 2$ , and 3), which are typical for lensed quasars. The curves in the

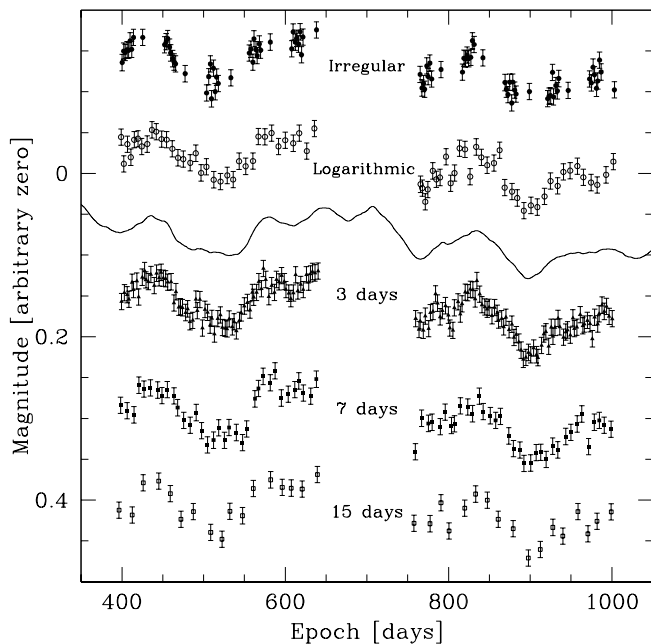


**Fig. 2.** Example of simulated light curve, for a 2-year long observation and a peak-to-peak amplitude  $A = 0.1$  mag. The continuous light curve is shown as a solid line. It has been smoothed on a length scale of 30 days. The four samplings used in the simulations are shown (plus the logarithmic sampling, see text), along with the error bars of 0.01 mag. The figure is constructed for an object with a visibility of 8 consecutive months, hence the size of the gap in the center of the curves is 4 months. The curve plotted for the logarithmic sampling has the same number of data points as the curve for the 7-day sampling.

figure show a variation time-scale of 10 to 100 days for a typical change of a few tenths of a magnitude. Realistic simulated light curves should show a time-scale for the variations, and a total “peak-to-peak” amplitude  $A = \delta m$  of the variation that are in accord with these results.

In order to mimic these variations we first consider a time series of  $N$  points spanning the total duration of the observation. For each of these points we define a simulated magnitude in such a way that the artificial light curve follows a random walk with an arbitrary peak-to-peak amplitude. We next smooth the light curve with a Gaussian kernel that has a Full-Width-Half-Maximum (FWHM) of 30 days to ensure that the typical variation time-scale matches that of real quasars. Finally, the curve is renormalized so that its maximum variation is equal to a specified peak-to-peak amplitude  $A$ .

A second light curve is then obtained, by applying a time shift  $\Delta t_{in} > 0$ . The two sets of points  $(t_A, m_A)$  for image A and  $(t_B, m_B)$  for image B obtained in this way are the final simulated light curves, both sampled with 10 points per 24 hours. This sampling, very small compared with the sampling that will be adopted to carry out the actual observations, ensures that no interpolation is necessary when shifting curve B relative to curve A. The

precision on the shift is, then, 0.1 day, 50 times smaller than the smallest time delay we wish to simulate.

The curves are used to produce artificial observations, this time with a much sparser sampling. We define  $N_{obs}$  observing points at the observing dates  $t_{obs}$ . For each of these dates we define the observed magnitude by selecting the closest value in time among the pairs  $(t_A, m_A)$  for image A and  $(t_B, m_B)$  for image B, resulting in noise free, sampled, artificial light curves. Finally, simulated photon noise is added to the data. This is achieved by adding to each observing point a normally distributed deviate of zero mean and variance  $\sigma_{obs}$ . Thus one has defined a combined set of  $N_{obs}$  observations,  $(t_{obs}, m_{A,obs})$  for image A and  $(t_{obs}, m_{B,obs})$  for image B. Typical light curves are shown in Fig. 2.

### 3. Parameter space

In the simulations presented below, some parameters are imposed on us by technical limitations. This is the case of the maximum accuracy on the photometry of the individual quasar images. We assume that a good goal is 0.01 mag for a typical lensed quasar, or a signal-to-noise of 100 integrated over the quasar image. We have tested some cases where the points have larger error bars, and this led to the conclusion that the adopted 0.01 mag error is a requirement to meet in order to carry out the project successfully. Doubling the error bars also doubles the error on the time-delay determination. Errors above 0.05 are likely to compromise the whole feasibility of the project. We also suppose that the algorithm used to carry out the photometry on the real data actually yields photon noise limited measurements. Second, we fix the total duration of the observations to two years, since one probably wants to measure  $H_0$  in a reasonable amount of telescope time.

Other parameters cannot be fixed in advance. They define the parameter space we want to explore through the simulations, and include:

1. The temporal sampling of the curves. We consider regularly spaced sampling intervals of 3, 7, and 15 days ( $\pm 30\%$  due, e.g., to bad weather). Also, in some observatories, large chunks of time are allocated rather than regularly spaced dates. To model this, as an example, we also carry out our experiment with a sampling of one observing point taken every other day during 15 days, followed by 1 single point taken in the middle of the next month, and again one point every other day for 15 days, and so on. We refer to this type of sampling as “irregular sampling”.
2. The visibility of the object. An equatorial object is seen no more than 5 months in a row in good conditions. A circumpolar object is by definition visible the entire year. We also choose an intermediate visibility of 8 months. It should be noted that we do not allow for large losses of data points, e.g. non allocation of time to the project during a full semester, which would simply hamper even a rough estimate of the time delay.

3. The amplitude  $A$  of variation of the quasar. We choose three typical peak-to-peak variations of  $A = 0.1, 0.2, 0.3$  mag over the two years of simulated observations, as suggested by Fig. 1.

Determining the best combination of these parameters is the goal of the present work, for a broad range of time delays, from 5 to 120 days. For each time delay there are 4 temporal samplings  $\times$  3 visibilities  $\times$  3 amplitudes = 36 different possible combinations of parameters.

#### 4. Extracting the time delay

Using the light curves constructed in the previous section, we now try to recover the time delay  $\Delta t_{in}$  chosen in the simulated data. Many cross-correlation techniques are available for this task, with a variety of technical subtleties dealing with unstable solutions, sparse sampling, and the effects of additional perturbations to the light curves (such as those caused by microlensing).

The aim of the present experiment is to decide which observing strategy will assure us that the present typical 10% error bar on optical time delays decreases below 2%, rather than testing the cross-correlation techniques themselves. For this reason, without further discussion, we have adopted the cross-correlation method of Pelt et al. (1994), which is in wide use, and which combines robustness, simplicity, and low cost in terms of computing time. No other correlation technique was used in the present simulations. More elaborated methods may be more efficient, so that our results can be considered as lower limits on the accuracy that can be actually achieved using a given set of light curves.

Although the Pelt method is well known, we briefly review the main steps followed to determine the time delay.

We first define an interval of time delays  $[\Delta t_{min}, \Delta t_{max}]$ , which contains the true value of the time delay  $\Delta t_{in}$ . Note that with real data, predicted time delays for lenses are accurate enough to follow this approach, especially in cases where the redshifts of the lens and source are known. We then define  $N_d$  equally spaced time delays over the range  $[\Delta t_{min}, \Delta t_{max}]$ , with interval  $\leq 0.1$  days i.e.  $N_d \geq (\Delta t_{max} - \Delta t_{min})/0.1 + 1$ . The interval is small compared with the input time delay  $\Delta t_{in}$  and ensures that the precision of the results, even for  $\Delta t_{in} = 5$  days, is not limited by the time resolution adopted in the simulations.

The light curve of image B is then shifted, successively, through the set of  $N_d$  time delays,  $\Delta t$ . The problem is to find which curve  $B(\Delta t)$  best matches curve A, within the overlap region. For any curve  $B(\Delta t)$  the overlap region is defined as the set of points for which there exist points in curve A, both before and after in time. Curve A is then linearly interpolated to these points, and the dispersion  $D^2(\Delta t)$  in the magnitude differences between the two curves provides the measure of goodness of fit. Data points for which the distance from the interpolated date to the closest date in curve A, is greater than some specified limit

(i.e. where the interpolation is unreliable) are ignored in this calculation. The search is limited, obviously, to time delays for which there is overlap of the two curves. Time delays of the order of half a year are thus only accessible for circumpolar objects.

This procedure yields the dispersion spectrum  $D^2(\Delta t)$ . The true time delay  $\Delta t_{out}$  between the images should be evident as a minimum in the dispersion spectrum  $D^2(\Delta t)$ . This minimum is determined by fitting a parabola to the dispersion spectrum.

#### 5. Results

For every time delay  $\Delta t_{in}$  to be simulated, we explored the full range of 36 different combinations of the three parameters, detailed in section 3. For each combination, we ran 100,000 simulations, each time changing the quasar light curve, and modifying the observed points by adding randomly distributed errors (i.e. normally distributed deviates of 0.01 mag variance). The results for  $\Delta t_{in} = 80$  days are summarized in Fig. 3, where the 36 panels correspond to the different parameter combinations. In each panel the measured time delays of the simulations are plotted in histogram form, with the measured mean and standard deviation (established by computing the range containing 68 % of the results) quoted. The histograms are mostly symmetrical about their mean value, indicating that no strong systematic error is introduced. The slight shift (0.5 days in the worst case) of the mean of the histogram relative to value of  $\Delta t_{in}$  is small compared with the width of the histogram, i.e., the random error dominate the error budget.

The results for the percentage error, for the 36 parameter combinations, for all the simulated time delays, are presented in a compact way in Fig. 4. Here each panel shows the results for 12 parameter combinations, which are the 4 temporal samplings  $\times$  the 3 visibilities, and the three columns correspond to the 3 amplitudes. Each row is for a different time delay. In this figure are also shown the values of the quoted relative errors for six published time delays of quasars monitored in optical wavelengths. These values are summarized in Table 1, and have been plotted at a sampling of 15 days, which roughly correspond to their effective sampling. Although the observational strategy used for these quasars is not strictly the same as any of the ones we have defined, the predicted errors lie rather close to the real ones, with the exception of the double quasar HE 2149-2745, but this quasar had very smooth variations over the two years of observations, much smoother than the typical variations used in our simulations (see Fig. 2). We do not include the twin quasar Q 0957+561 because it has a 10-year long light curve, much longer than the two years considered in our simulations. Moreover its time delay of  $423 \pm 6$  days (Pelt et al. 1996) is much larger than the highest time delay used (i.e. 120 days).

Although the predicted relative errors on the time delay are very close to the published values, they are usually

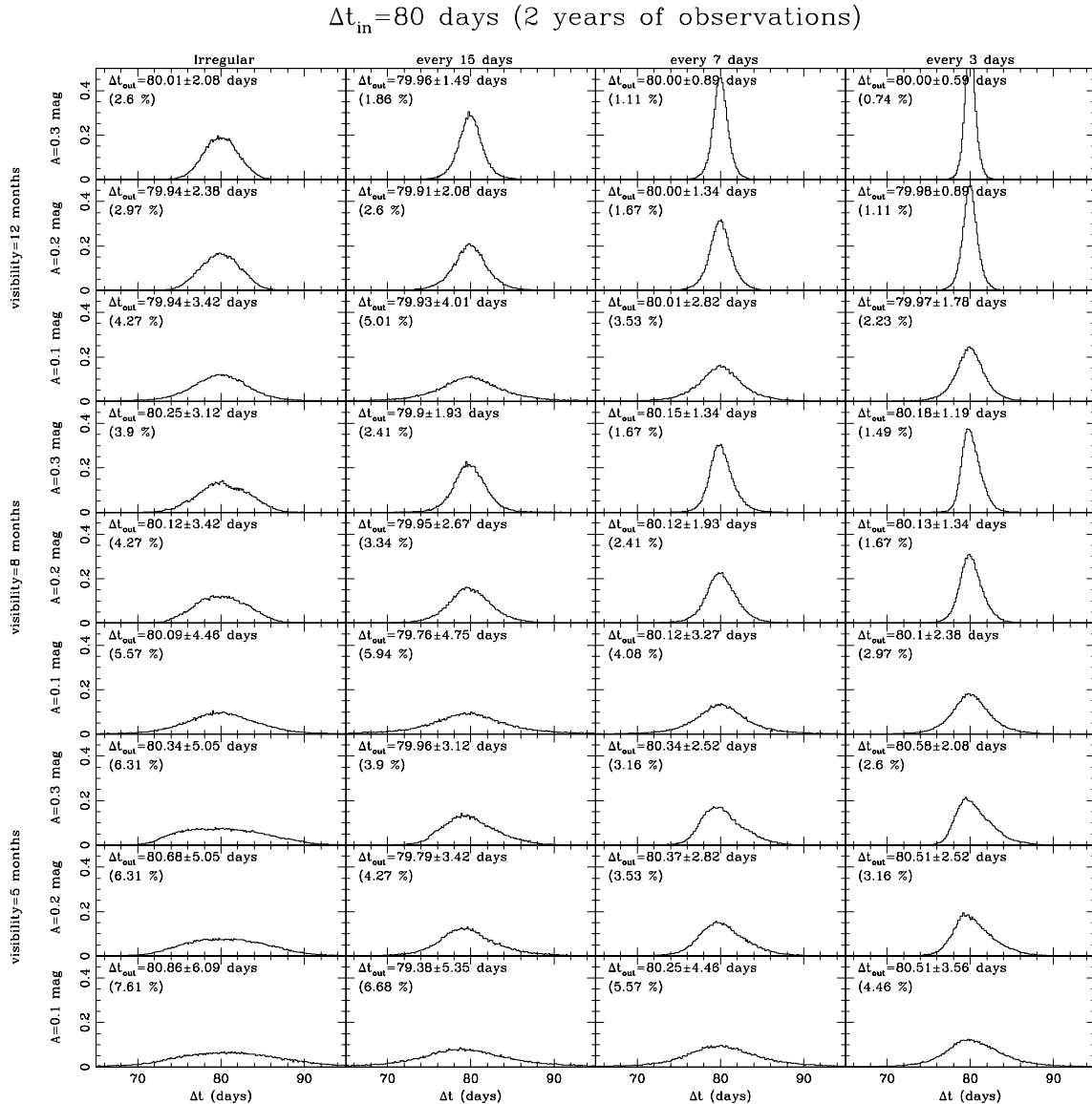


**Fig. 3.** Histograms exploring the observational parameter space described in the text for the determination of a time delay of 80 days. Each curve is the probability density function for the time delay, obtained from 100,000 simulations, for a particular combination of the three variables. These are: **1-** *sampling interval*, four columns, from left to right: irregular, 15 days, 7 days, 3 days); **2-** *visibility period*, three bands from top to bottom: 12, 8, and 5 months; **3-** *peak-to-peak variation*,  $A$ , three rows within each band, from top to bottom: 0.3, 0.2, 0.1 mag. Each panel is labeled with the mean and standard deviation of the measured time delay, as well as the percentage error. The effect of microlensing is not included in these simulations, and is treated later.

slightly more optimistic than the measured relative errors. The small discrepancies can be explained by differences in the parameters we use, compared with the characteristics of actual monitoring data, e.g.:

- a shorter or longer monitoring period than the supposed two years,
- different photometric errors than the supposed 0.01 mag,
- a temporal sampling that differs in detail from our idealized scheme.

The most likely explanation for the simulations being too optimistic however remains the presence of microlensing in the light curves of real quasars, which is the subject of the next section.

## 6. Influence of “slow” microlensing

Not all the photometric variations observed in the light curves of the quasar images are intrinsic to the quasar. Microlensing by stars in the lensing galaxy introduces amplification events that contaminate the light curves.

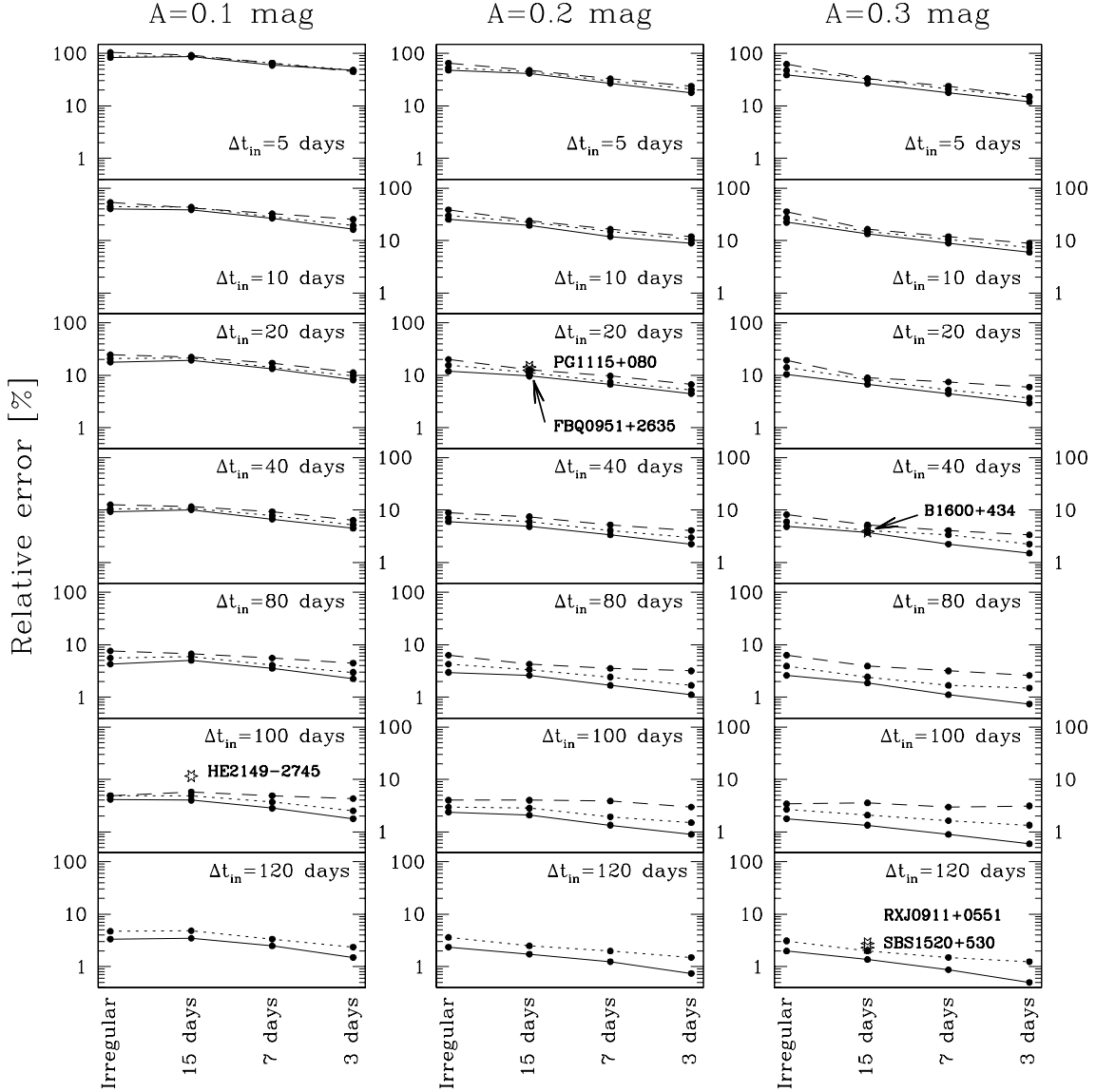


**Fig. 4.** Summary of the estimated percentage error on the measured time delay as a function of the observational parameters: **1-** *peak-to-peak variation*,  $A$ ; **2-** *sampling interval* (x-axis of each panel); **3-** *visibility period*. Each panel corresponds to one value of the input time delay  $\Delta t_{in}$ . The percentage error on the time delay, plotted on the y-axis, is calculated from 100,000 simulations. The lines connecting the points correspond to different periods of visibility. The solid lines are for circumpolar objects, the dotted lines are for the 8-month visibility, and the long dashed lines are for the 5-month visibility. We have used three peak-to-peak values of the amplitudes  $A$  for the simulated light curves, which increases from left to right in the three columns. The curve for the 5-month visibility and 120-day time delay has not been computed, as there are almost no data points in common between the curves of image A and image B. The star-shaped symbols plot the percentage errors for quasars with real measured optical time delays published in the literature. See text for further details.

The severity of such events depends not only on the location of the images relative to the lens but also on whether the image considered is a minimum, maximum or a saddle point in the arrival time surface (Schechter & Wambsganss 2002). Consequently, the image closest to the lens, in projection on the plane of the sky, and hence with the larger density of potential microlenses, is not necessarily the one with more microlensing. The doubly lensed quasar HE 1104-1805 is a typical example, where the im-

age the further away from the lens is the one with the largest microlensing events.

Microlensing can act on different time scales, “slow” or “fast”, as compared with the time scale of the quasar’s intrinsic variations. A nice example of fast microlensing has been found in the light curve of HE 1104-1805 (e.g., Schechter et al. 2003). Since the temporal sampling used in past quasar monitoring programmes has been rather sparse, there is no other known example of fast microlens-

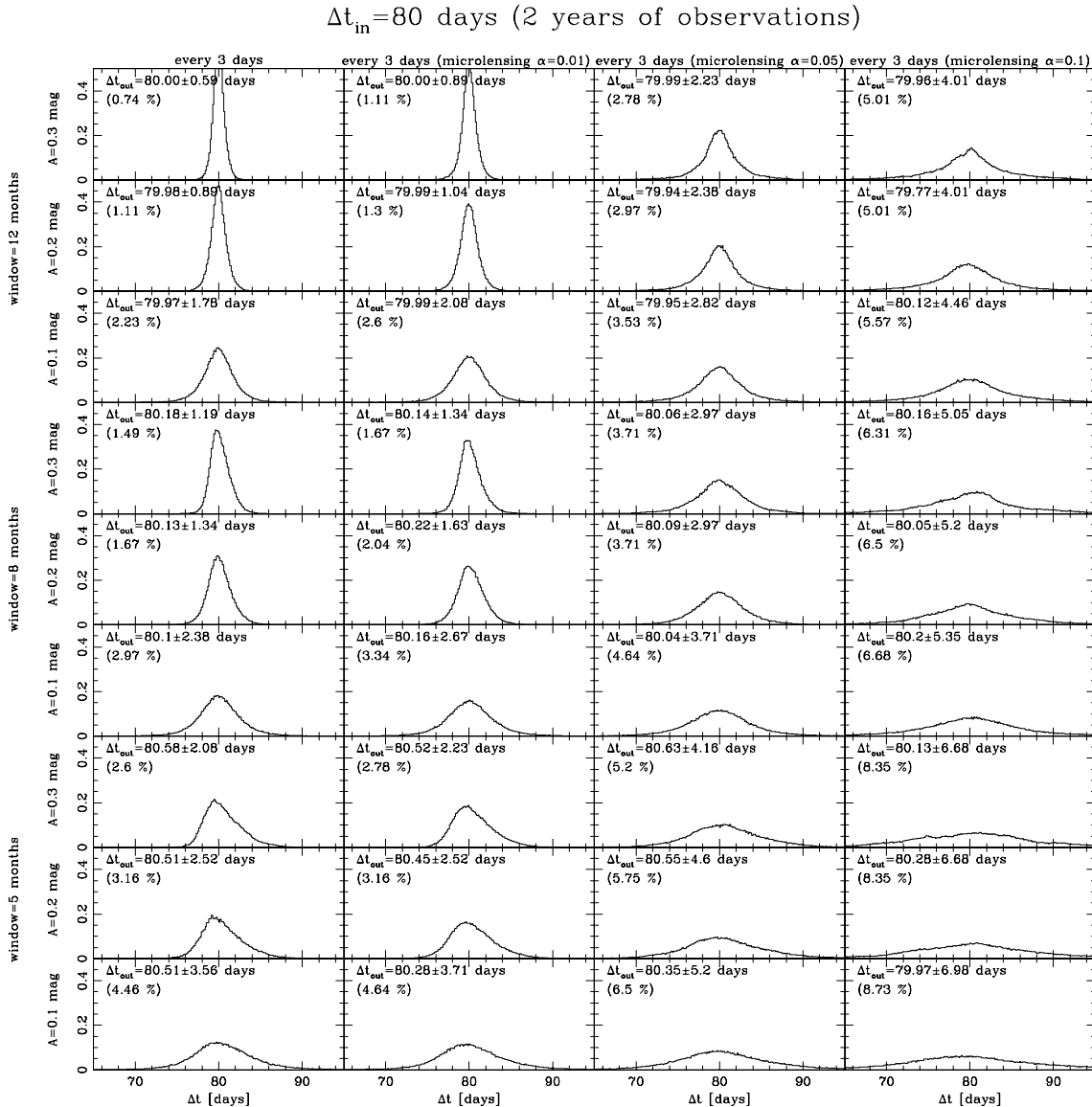


**Fig. 5.** Histograms exploring the observational parameter space described in the text for the determination of a time delay of 80 days, including the effects of microlensing. Each curve is the probability density function for the time delay, obtained from 100,000 simulations, for a sampling interval of 3 days, and for a particular combination of the variables. These are: **1-** *microlensing amplitude*,  $A_\mu = \alpha \cdot A$ , four columns, from left to right:  $\alpha = 0, 0.01, 0.05, 0.1$ ; **2-** *visibility period*, three bands from top to bottom: 12, 8, and 5 months); **3-** *peak-to-peak variation*,  $A$ , three rows within each band, from top to bottom: 0.3, 0.2, 0.1 mag. Each panel is labeled with the mean and standard deviation of the measured time delay, as well as the percentage error. While no strong systematic drifts of the histograms are seen relative to the input time delay  $\Delta t_{in} = 80$  days, the width of the histograms are significantly broadened as microlensing increases.

ing. Slow microlensing, with smooth variations spanning several months or even years are more common, or are at least better detected with existing data. The slow variations in the four images of the Einstein Cross are the clearest examples of slow microlensing (e.g., Wozniak et al. 2000).

Since most quasars with measured time delays have been shown to be affected by slow microlensing, it is mandatory to introduce this effect into our artificial light curves and to estimate how the time-delay measurement

is modified. The slow microlensing events can be simulated by creating a *microlensing* light curve in the same manner as we did for the intrinsic variations of the quasar (i.e. by using a smooth random walk model), but with a different length scale and amplitude. We express the peak-to-peak microlensing amplitude  $A_\mu$  as a simple function of the quasar amplitude. We take it as  $A_\mu = \alpha \cdot A$ , with  $\alpha = 0.01, 0.05, 0.10$ , in order to mimic a microlensing amplitude of respectively 1, 5 and 10% of the amplitude of the quasar light curve. The microlensing curve is smoothed us-

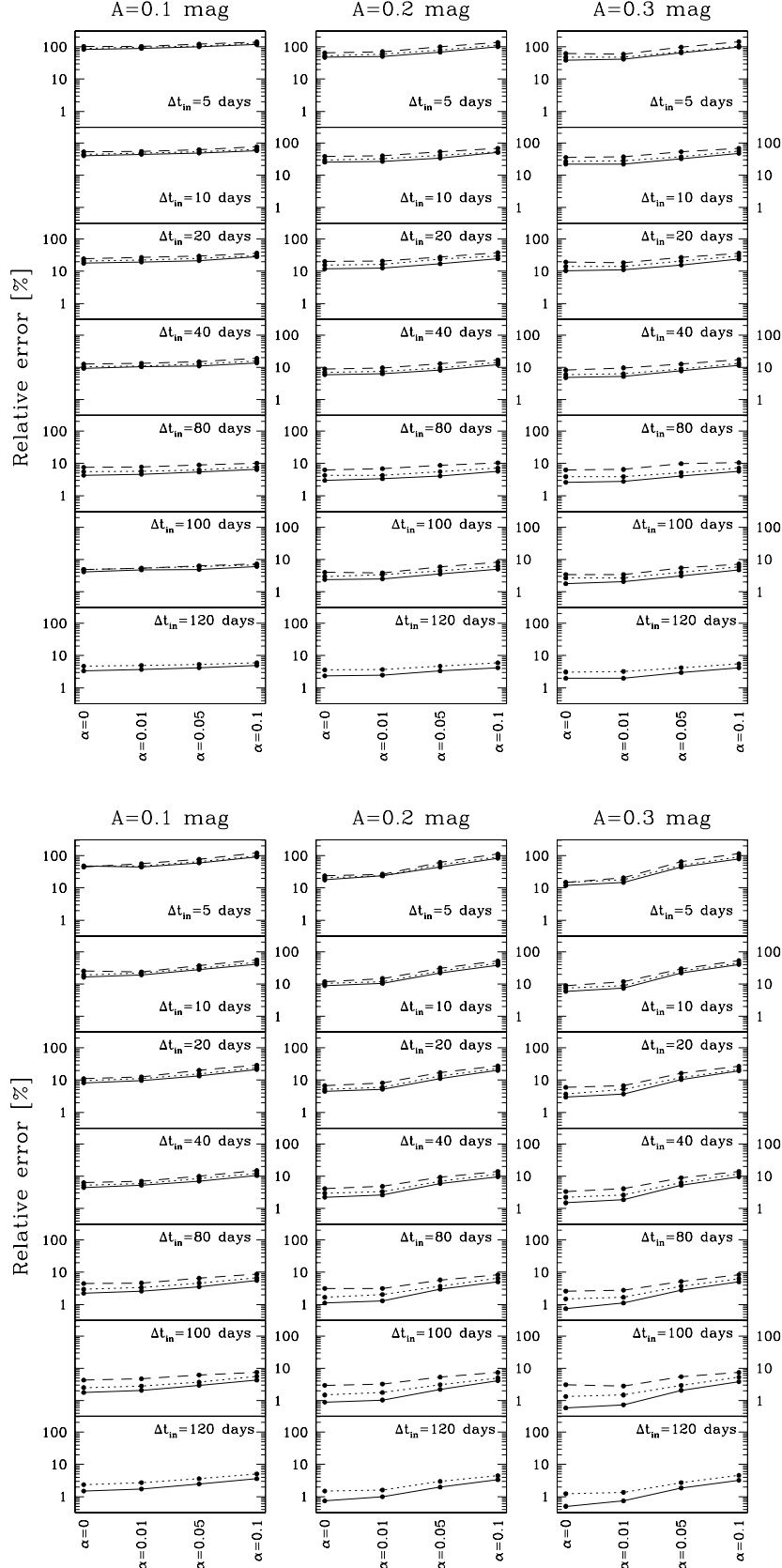


**Fig. 6.** *Top:* Percentage error on the time delay for the *irregular sampling* and for three amplitudes  $A$ . In each column the results are shown for four microlensing amplitudes  $A_\mu = \alpha \cdot A$ , starting on the left with  $\alpha = 0$ , i.e., no microlensing. The different types of curves correspond to the three visibilities, as in Fig. 4. The solid lines are for circumpolar objects, the dotted lines are for the 8-month visibility, and the long dashed lines are for the 5-month visibility. *Bottom:* same

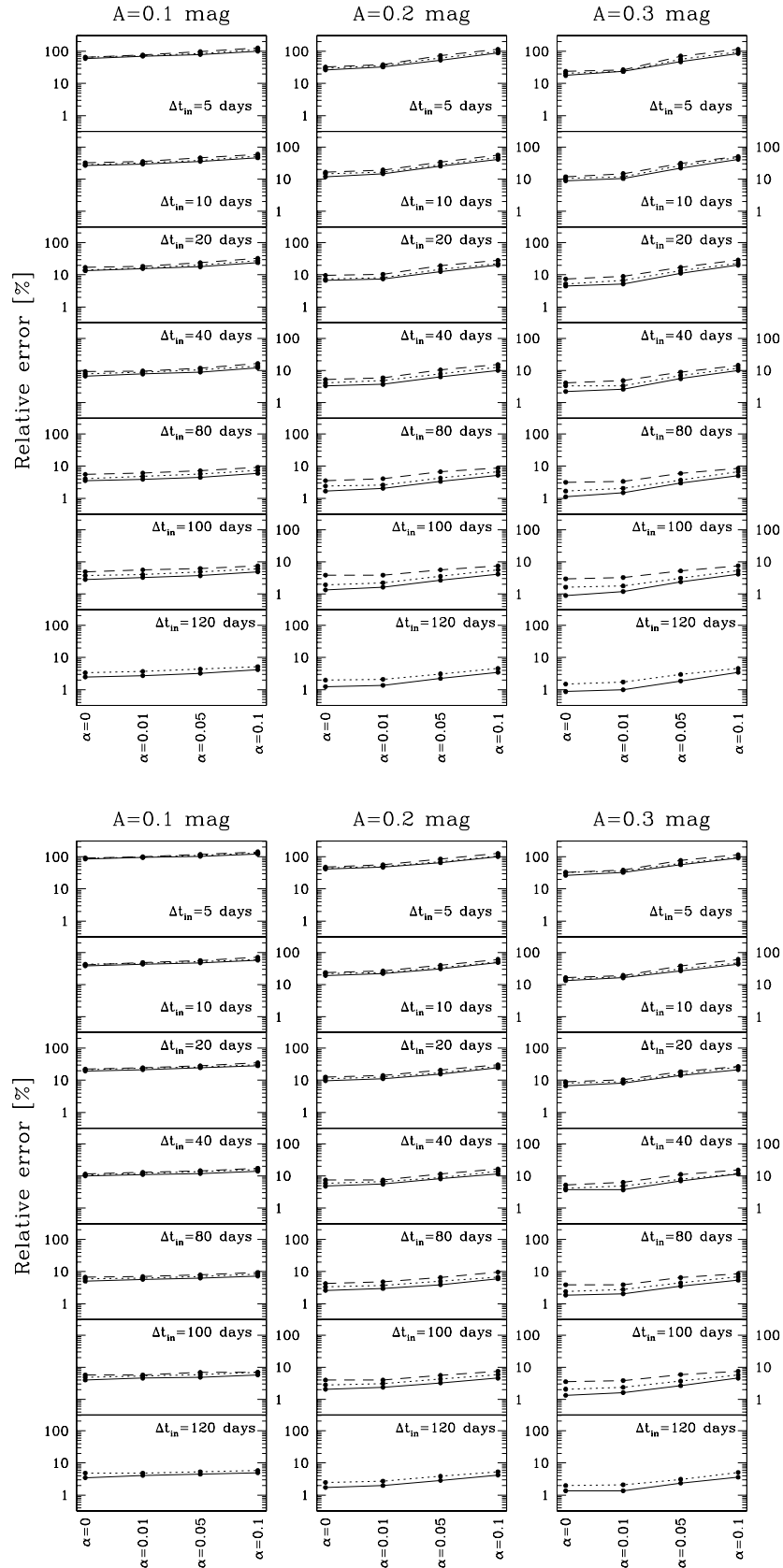


Fig. 7. Same as Fig. 6, but for the 7-day sampling (top) and for the 15-day sampling (bottom).

**Table 1.** Published time delays and  $1\text{-}\sigma$  uncertainties for four lensed quasars, measured from their optical light curves. The percentage errors are given in parentheses.

Object	Time delay [days]	Reference
RXJ 0911+0551	$146 \pm 4$ (2.7%)	Hjorth et al. 2002
FBQ 0951+2635	$16 \pm 2$ (13%)	Jakobsson et al. 2004
PG 1115+080	$23.7 \pm 3.4$ (14%)	Schechter et al. 1997
SBS 1520+530	$130 \pm 3$ (2.3%)	Burud et al. 2002a
B 1600+434	$51 \pm 2$ (3.9%)	Burud et al. 2000
HE 2149-2745	$103 \pm 12$ (12%)	Burud et al. 2002b

ing a convolution kernel of 100 days, i.e.  $\sim 3$  times slower than the intrinsic variations of the quasar, and is added to the light curve of one of the quasar images. The choice of this image is irrelevant, because only relative differences between the lightcurves of the two components are considered to extract the time delay.

We then repeat the cross-correlation analysis. The microlensing event, thus, acts as an additional source of noise. Fast microlensing is not considered here. Introducing it is equivalent to artificially increase the 0.01 mag error bar on the individual points.

Fig. 5 plots the results for the case of the 80-day time delay, and 3-day sampling, with different amplitudes of microlensing. The format is the same as in Fig. 3. It can be seen that no strong systematic variations are introduced. In each case the returned time delay is consistent with the input value, but microlensing substantially increases the uncertainty in the measurement, i.e. broadens the histograms. No distortion, i.e., skewness is apparent. The error on the time delay measurement without microlensing (left column) typically degrades by a factor of approximately 2 when 5% microlensing is present (i.e.,  $\alpha = 0.05$ ), and by up to a factor of 6 with 10% microlensing. However, the shift between the mean of the distribution and  $\Delta t_{in}$  is not much larger than in the no-microlensing case. Slow microlensing does not seem to introduce significant systematic errors.

Figs. 6 and 7 summarize all the results of our simulations including microlensing, in a way similar to Fig. 4, showing how the error on the time delay degrades with increasing microlensing amplitude ( $\alpha$ , plotted on the x-axis in each of the column plots). The figures are constructed for the irregular sampling as well as for the regular 3-day, 7-day and 15-day samplings.

We note that the time-delay determination is much more affected by microlensing with the 3-day sampling than with the 15-day or the "irregular" samplings: while changing  $\alpha$  from 0 to 0.1 increases the relative error by a factor of 8 for the 3-day sampling, it increases only by a factor of 3-4 with the 15-day or the irregular sampling. Microlensing has a stronger effect on well sampled light curves than on sparser samplings.

Similarly a light curve with large amplitude  $A$  will see its accuracy on the time-delay measurement slightly more degraded than one with a smaller amplitude. In both cases this may simply be due to the enhanced signal-to-noise of the light curves, either because more data points are available, or because the quasar variations are stronger with respect to the photon noise of the individual photometric points.

In general we can conclude that the more accurate the time-delay determination is in the case without microlensing, the more it degrades when a given amount  $\alpha$  of microlensing is added: better data are more sensitive to microlensing. On the other hand, the data allowing accurate time delay determinations in the absence of microlensing are usually also better suited to the accurate subtraction of the microlensing events.

## 7. When the time delay becomes close to the length of the visibility window

So far we have compared light curves sampled with regular samplings, plus one irregular sampling. The main difference between these samplings was the number of data points within the period of 2 years of observations. It is then not surprising that finer sampling leads to better results. The simulations we have done allow us to quantify the error bar on the time delay for each sampling.

Another natural question arising is: is there an optimal way to distribute a fixed number of sampling points, in order to reach the best possible accuracy on the time delay? This has been explored in other areas of astronomy, for example by adopting a logarithmic sampling of the data. We have tested the effect of such a sampling on quasar light curves. Fig. 8 shows the results of the simulations, where we compare the (regular) 7-day sampling to a sampling adopting the exact same number of data points but distributed in a logarithmic way. As for the regular case, we have introduced a small randomly distributed error ( $\pm 0.4$  days) on each observing data to account for weather conditions and scheduling. As shown in Fig. 2 the curve starts with a very high frequency of observations and continues with a sampling getting close to regular. An important consequence is that objects that have a time delay of the order of the visibility period will be well sampled exactly where the two quasar light curves significantly overlap after correcting for the time delay. In other words, the logarithmic scale allows to sample very well the (short) parts of the curves that will overlap after the time delay is applied.

The result in Fig. 8 is striking. As soon as the time delay is close to the length of the visibility window, the regular method fails to produce symmetrical histograms, whereas the histograms obtained with the logarithmic scale are narrower and more symmetrical about their mean. Their mean is also closer to  $\Delta t_{in}$  than with the regular method. This is no longer true when the time delay is shorter than the visibility window, where the logarithmic sampling even degrades the results.

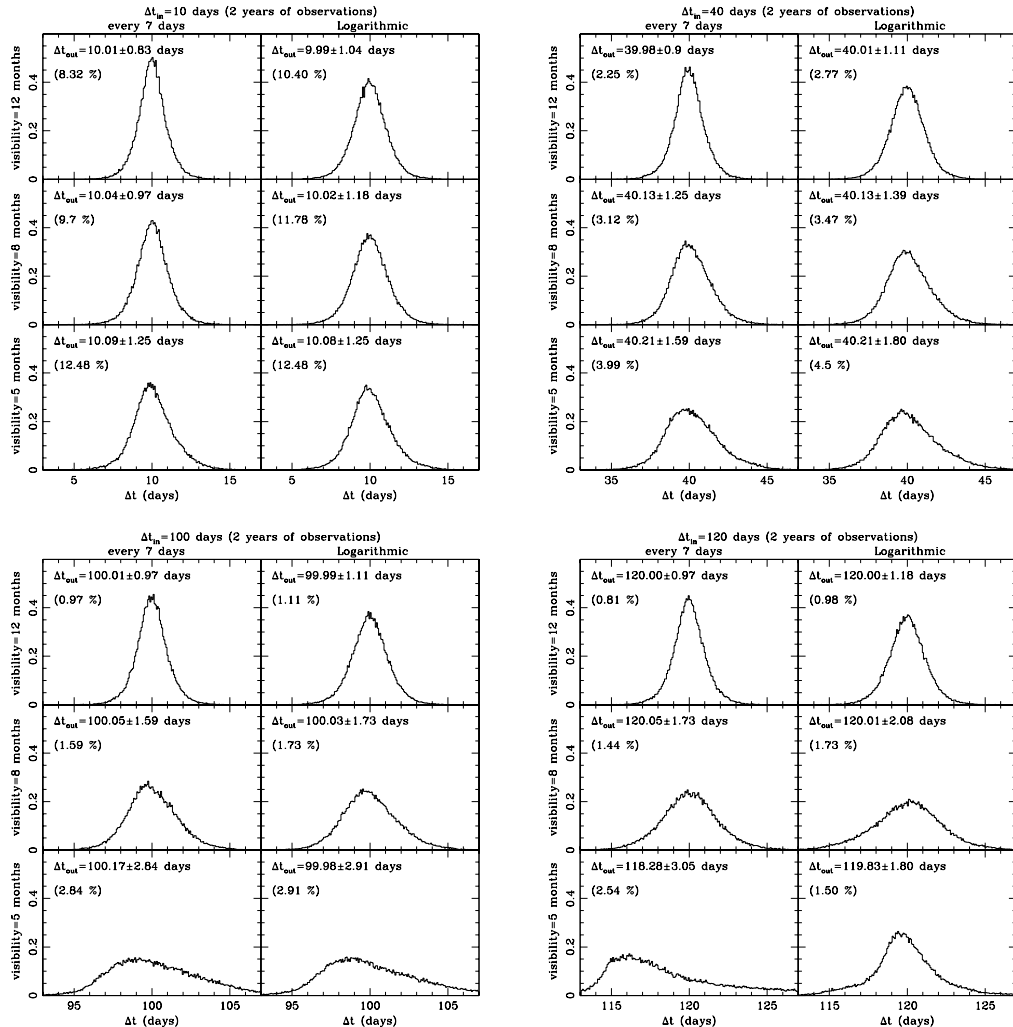


**Fig. 8.** Time delay distributions for four different values of  $\Delta t_{in}$ , each time for 3 visibilities and a peak-to-peak variation  $A = 0.3$ . We compare the distributions obtained for the logarithmic sampling (without microlensing), with the results for the 7-day sampling. Clear distortions of the histograms are seen when the time delay is close to the visibility window of the object, when a regular sampling is adopted (left column in the four panels). The histograms obtained with the logarithmic sampling are well symmetrical and narrow. The systematic error is also reduced. This effect is not so evident when the time delay is much shorter than the visibility window, where the logarithmic sampling even degrades the results.

## 8. Conclusions

We have undertaken a set of simple but realistic numerical simulations in order to optimize the observing strategy of our COSMOGRAIL photometric monitoring programs aimed at measuring  $H_0$ . The predicted error bars on time delays compare very well with the ones obtained in optical wavelengths with real data.

It is immediately seen from Figs. 6 and 7 that short time delays will never be measured accurately, i.e., with a precision better than 2%, unless the quasar amplitude  $A$  is substantially larger than 0.3 mag. Even with no microlensing and the 3-day sampling, time delays shorter than 10 days are measurable with 10% accuracy, at best. Time delays between 40 and 100 days seem optimal, especially

in the case of circumpolar objects, where one can easily achieve 2% accuracy, even with the 7-day sampling.

Equatorial objects should be avoided. Although they are accessible from the north and south, they are visible under good conditions for only 5-6 months along the year. This makes it impossible to measure time delays larger than 100 days (hence the corresponding long-dashed curve is not represented in the relevant figures). For shorter time delays, e.g., 80 days, the estimated error for an equatorial object is twice that of the same object if it were circumpolar.

Microlensing complicates the situation. With 5% microlensing (as defined here), the estimated error on the time delay is twice that of the no-microlensing case. Again, optimal time delays are around 100 days, with a visibil-

ity of at least 8 months. Assuming an amplitude  $A = 0.2$  magnitude and 5% microlensing, an accuracy of 2% on the time delay is still possible for these objects. The long time delays also allow a sampling as long as 7 days to be adopted.

While microlensing increases the random error on the time delay, it does not increase significantly the systematic error (i.e.,  $|\Delta t_{in} - \Delta t_{out}|$ ), which remains low, usually 5 to 10 times lower than the random error, with or without microlensing.

Finally, adopting a logarithmic sampling step can improve the accuracy on the time delay when the time delay is close to the length of the visibility window of the object. However, this logarithmic sampling usually degrades the results for all other combinations of time delays and visibility windows.

The game of defining what could be a “golden” lens, at least in terms of quality of the time delay measurement, is not an easy one. This is why we have attempted in this paper to provide a grid of predicted error bars on the time delay, based on simple assumptions. The results are presented in a compact way in Figs. 6 and Figs. 7. We will use these plots to choose optimal combinations of **1-** predicted time delay, **2-** object visibility and **3-** temporal sampling, to reach a target accuracy on the time delay. Even with large amounts of telescope time, the number of new lensed quasars is increasing quickly and one has to select the best possible cases. We hope that the present work will be useful for the task of identifying the objects that are the most likely to be measured accurately, so that the only significant remaining source of uncertainty on  $H_0$  will be the lens model.

## References

- Burud, I., Hjorth, J., Courbin, F., et al. 2002, *A&A* 391, 481  
 Burud, I., Hjorth, J., Jaunsen, A. O., et al. 2000, *ApJ* 544, 117  
 Burud, I., Courbin, F., Magain, P., et al. 2002, *A&A* 383, 71  
 Colley, W., Schild, R. E., Abajas, C., et al. 2003, *ApJ* 587, 71  
 Fassnacht, C. D., Xanthopoulos, E., Koopmans, L. V. E., et al. 2002, *ApJ* 581, 823  
 Hjorth, J., Burud, I., Jaunsen, A. O., et al. 2002, *ApJ* 572, 11  
 Hook, I., et al. 1994, *MNRAS* 268, 305  
 Jakobsson, P., Hjorth, J., Burud, I., et al., astro-ph/0409444  
 Magain, P., Courbin, F., Sohy, S., 1998, *ApJ* 494, 452  
 Pelt, J., Hoff, W., Kayser, R., et al., 1994, *A&A* 286, 775  
 Pelt, J., Kayser, R., Refsdal, S., et al., 1996, *A&A* 305, 97  
 Refsdal, S. 1964, *MNRAS* 128, 307  
 Saha, P. et al. 2005, in preparation  
 Schechter, P. L., Bailyn, C. D., Barr, R., et al. 1997, *ApJ* 475, 85  
 Schechter, P. L., Udalski, A., Szymanski, M., et al. 2003, *ApJ* 584, 657  
 Schechter, P. L. & Wambsganss, J., 2002, *ApJ* 580, 685  
 Wozniak, P. R., Udalski, A., Szymanski, M., et al. 2000, *ApJ* 540, 65